https://doi.org/10.5194/egusphere-2026-3363
Preprint. Discussion started: 20 July 2026

Random forest predictions of tundra snow density elevate Arctic soil temperatures in CLM5.0

Johnny Rutherford[1], Nick Rutter[1], Leanne Wake[1], Georgina Woolley[1], Julia Boike[2,3] and Alex J. Cannon[4]

[1]Department of Geography and Environmental Sciences, Northumbria University, Newcastle Upon Tyne, UK.
[2]Permafrost Research, Geosciences, Alfred Wegener Institute, Helmholtz Centre for Polar and Marine Research, Telegrafenberg A45, Potsdam, 14473, Germany.
[3]Department of Geography, Humboldt-Universität zu Berlin, Berlin, Germany
[4]Climate Modelling Division, Environment and Climate Change Canada.

Correspondence to: Johnny A. D. Rutherford (Johnny.rutherford@northumbria.ac.uk)

Abstract

Arctic snow exerts a critical control on winter soil temperature and carbon exchange, however representation of its properties in Earth System Models (ESMs) remains simplified. In the Community Land Model v5.0 (CLM5.0), recent updates to snow compaction schemes have led to overly dense tundra snow, increasing snow thermal conductivity and conductive heat loss, producing a persistent cold-soil bias. Here we developed a Random Forest (RF) regression model to derive tundra bulk snow density from meteorological variables, trained on six winter seasons (Sep – May) of Arctic SVS2-Crocus (ASC) simulations constrained by in-situ observations from Trail Valley Creek (TVC), Northwest Territories, Canada. RF-derived snow densities capture the lower bulk densities of Arctic tundra snowpacks, which CLM5.0's compaction scheme overestimates. Application of the RF-derived snow densities to CLM5.0 reduces snow thermal conductivity and enhances snowpack insulation, decreasing soil temperature RMSE by approximately 2 – 3 °C relative to field measurements (2017 – 2023) and increasing future winter soil temperature projections (2016 – 2100) by 4 – 7 °C under RCP4.5 and 8.5. Such increases in simulated soil temperature highlight the strong sensitivity of CLM5.0's soil thermal regime to snow physical properties. The RF model reproduces ASC-simulated density evolution with a mean absolute error of 32 kg m^{-3} which falls within typical measurement error for volumetric snow density sampling in Arctic tundra (20 – 40) kg m^{-3} and matches field measurements more closely than default CLM5.0. Future bulk snow density predictions using the RF model driven by bias-corrected North American-Coordinated Regional Downscaling Experiment (NA-CORDEX) meteorology indicate bulk snow densities 200 – 450 kg m^{-3} lower than CLM5.0 and more consistent with tundra conditions.

1 Introduction

The Arctic is warming up to four times faster than the global average (Rantanen et al., 2022), risking the mobilisation of approximately 1700 GT carbon stored in permafrost systems and threatening to exacerbate the atmospheric carbon feedback (Miner et al., 2022). Arctic warming is particularly pronounced in winter, with temperatures estimated to warm by 4.8 °C by 2100 compared to 2.2 °C in the summer over the same period (Webb et al., 2016; Christensen et al., 2013). Snow is a key component of the Arctic system which directly influences

https://doi.org/10.5194/egusphere-2026-3363
Preprint. Discussion started: 20 July 2026

ground-atmosphere energy fluxes, soil temperature, and freeze-thaw state (Bigalke and Walsh, 2022; Mudryk et al., 2019; Mudryk et al., 2020; Cohen et al., 2015; Serreze et al., 2021; Trenberth, 1998). Thus, changes in Arctic snow properties due to a warming climate may drive shifts in wintertime soil temperature, with downstream implications to heterotrophic respiration and carbon release (CO_2 and CH_4) (Natali et al., 2019). Capturing evolving snowpack properties is vital for accurately modelling soil temperatures in Arctic tundra; however, Earth System Models (ESMs) remain limited in their representation of these processes (Rixen et al., 2022; Royer et al., 2021). Accurate modelling of soil temperatures in ESMs is increasingly important for soil carbon flux projections as soil CO_2 and CH_4 emissions are highly sensitive to temperature change (Natali et al., 2019). In this study, we focus on the Community Land Model version 5.0 (CLM5.0), a widely used land surface model within the Community Earth System Model (CESM), where deficiencies in tundra snow representation produce systematic biases in winter soil temperatures.

Poor representation of tundra snow in ESMs such as CLM5.0 results in an overestimation of thermal transfer between the atmosphere and Arctic soils. The update from CLM4.5 to CLM5.0 improved unrealistically low snow density over areas such as Antarctica and Greenland through better representation of firn and the transition from snow to ice (Lawrence et al., 2019). However, these updates, which focussed on improving surface mass balance over ice sheets, have had unintended consequences on simulated tundra snow where overly dense snow causes an overestimation in snowpack thermal conductivity. This overestimation produces a cold bias for simulated winter soil temperatures which propagate to future projections of winter carbon fluxes (Rutherford et al., 2025; Dutch et al., 2022; Damseaux et al., 2024). This deficiency reflects the absence of key snowpack processes that control tundra snow structure and thermal properties. Critically, the current snow schemes in ESMs, including CLM5.0 fail to represent interactions between vertical temperature gradients and vapour transport which are vital to the creation of depth hoar, a key component of tundra snow. In tundra environments basal depth hoar forms early in winter under large temperature gradients between the ground and overlying snow (Bouvet et al., 2023). As the season progresses, snow accumulates and Arctic winds densify upper layers into wind slab (Sturm et al., 1995; Derksen et al., 2009; Derksen et al., 2014). However, basal depth hoar is sustained throughout the winter, giving tundra snow characteristically low bulk density and this contributes significantly to the high insulative capacity of the snowpack. Wind slab layers have a typically high thermal conductivity of 0.15 – 0.5 W m^{-1} K^{-1} while depth hoar show much lower values, 0.025 – 0.1 W m^{-1} K^{-1} (Domine et al., 2018). Consequently, these shallow and highly abundant low-density snowpacks associated with shrub tundra environments are critical to the control of soil temperatures in permafrost environments and need to be represented in ESMs.

Currently, the overestimation of bulk snow density in ESMs directly affects heat transfer through the snowpack, as effective thermal conductivity (K_{eff}) increases with density. As such, understanding K_{eff} is critical to assessing the role of snow in the cryosphere in light of a changing climate (Calonne et al., 2011). The parameterisation of K_{eff} in models often considers only the conduction through ice and air within the snow and omits other factors such as phase change effects, vapour diffusion and air convection within pores (Calonne et al., 2011). Relationships between snow density and K_{eff} have been proposed by several studies and show K_{eff} increasing as a function of density (Calonne et al., 2011; Sturm et al., 1997; Fourteau et al., 2021). Sturm et al. (1997) introduces a scheme that considers lower density snow types such as depth hoar and when applied in CLM5.0 significantly impacts projected future carbon emissions from Arctic soils (Rutherford et al., 2025). While the Sturm scheme

https://doi.org/10.5194/egusphere-2026-3363
Preprint. Discussion started: 20 July 2026

accounts for cold biases in winter soil temperature, it does so because the K_{eff} parameterisation counteracts the effect of overly dense snow. However, this does not address the underlying issue of overly dense snow caused by omission of depth hoar formation in simulated seasonal snow in CLM5.0 as identified by Damseaux et al. (2024) and Dutch et al. (2022). An alternative approach is therefore needed to derive bulk snow density that captures the physical processes driving tundra snowpack evolution without relying on CLM5.0's compaction scheme.

The representation of tundra snow processes in ESMs remains simplified, due to complex and nonlinear interactions between meteorology, topography, and vegetation (Wang et al., 2023). These simplifications highlight the need for alternative approaches that can capture the complex, nonlinear controls on snow density without relying solely on simplified physical parameterisations. Random forest (RF) regression models can both capture complex non-linear relationships more effectively than linear models and incorporate a broad range of predictor variables which can include categoric information such as topographic features and vegetation cover. Such RF approaches have shown to be promising tools for the estimation of snow depth from predictor inputs such as topographic position, satellite brightness temperature, geographic location, elevation and land cover fraction (Revuelto et al., 2020; Meloche et al., 2022; Yang et al., 2020). Further, RF scores well alongside other machine learning (ML) approaches for predicting snow density and snow water equivalent (SWE) from site specific variables, including elevation, slope, and aspect, as well as meteorological information such as near-surface air temperature and wind speed (Goodarzi et al., 2024; Kanda and Fletcher, 2025). Despite known limitations, RF modelling offers a promising approach for bulk snow density prediction which builds on the statistical approach developed by Meløysund et al. (2007) using meteorological predictors.

While several studies deploy RF algorithms for snow depth estimation (Revuelto et al., 2020; Meloche et al., 2022; Gunn et al., 2025), applications to snow density remain limited in number. Notably, Prasad et al. (2024) explored several machine learning methods including RF to emulate the physically based snow model 'SnowModel' with applications to snow density predictions on sea ice. In contrast, our study focused on snow density prediction for terrestrial tundra (Thompson et al., 2016), which play a critical role in regulating soil temperatures which influence permafrost stability and carbon release (Zhang, 2005). Tundra snowpacks are characterised by thick wind slab layers and low density depth hoar which greatly influences the insulation of soils (Sturm et al., 2001; Domine et al., 2015). By contrast, snow on sea ice is generally thinner than terrestrial tundra due to wind compaction and redistribution, and is characterised by higher density depth hoar layers (Sturm et al., 2002). Consequently, RF models developed for sea-ice snowpacks may not adequately represent the density evolution and thermal impacts of tundra snow. Capturing tundra snowpack characteristics is therefore important for improving land-atmosphere simulations in a rapidly changing Arctic.

Training a RF requires a sufficiently large training dataset to allow the model to robustly learn relationships between meteorological drivers and bulk snow density (Breiman, 2001). However, in-situ measurements of Arctic tundra snow properties are very sparse in location and continuity (Stuefer et al., 2025), as field campaigns are often conducted at or near peak SWE (Apr – May). An alternative data source is therefore required for season long bulk snow density data for training a RF model. Arctic SVS2-Crocus (ASC) is a multi-physics ensemble version of the Crocus snowpack model embedded within the Soil, Vegetation, and Snow model version 2, with Arctic-specific parameterisations of wind-induced compaction, basal vegetation effects, and thermal conductivity implementation to improve the simulation of snow density profiles at tundra sites (Vionnet et al., 2025; Woolley

https://doi.org/10.5194/egusphere-2026-3363
Preprint. Discussion started: 20 July 2026

et al., 2024). The 120-member ensemble framework provides a diverse set of physically plausible density realisations which span a range of processes representations. When evaluated over 32 years (1991 – 2023) at Trail Valley Creek, NWT, Canada, ASC demonstrated improved simulation of snow density profiles relative to the default model configuration. ASC reduced RMSE in wind slab by 41% and produced more physically representative profiles of low-density basal layers overlying high density surface layers (Woolley et al., 2024). Given its performance at TVC and its ability to generate physically plausible season-long bulk snow density simulations, ASC outputs complement sparse field observations for training a RF model at this site. While a RF model trained on ASC may inherit model-specific biases, the physically constrained ensemble framework offers a practical solution to expanding a RF training dataset given the sparsity of observational data.

This study assesses the capacity of RF predicted bulk snow densities to improve snow thermal conductivity parameterisation and soil temperature simulations in CLM5.0. Firstly, an RF model is developed to capture patterns in seasonal bulk snow density as simulated by ASC, and RF predictions are compared against default CLM5.0 bulk snow density outputs and field measurements taken at TVC during peak SWE (April – May). The RF bulk snow density predictions are then inserted to CLM5.0 and tested in present-day conditions (2017 – 2023) and simulated soil temperatures are compared with field measurements at 10 cm and 2 m depth. Finally, future bulk snow density estimates (2016 – 2100) produced by the RF model are compared with those of default CLM5.0 and are applied to future simulations to assess the impact of bulk snow density on future soil temperatures under Representative Concentration Pathways (RCP) 4.5 and 8.5.

2 Methodology

2.1 Study site

TVC is a research watershed located approximately 50km north of Inuvik, NWT, Canada, in the tundra-taiga ecotone with vegetation consisting mainly of low shrubs, lichens, grasses and mosses (Marsh et al., 2010; King et al., 2018). Snow cover in the TVC watershed varies spatially due to topography, wind re-distribution and vegetation cover (Pomeroy et al., 1993; Derksen et al., 2014; King et al., 2018; Wilcox et al., 2019). In-situ measurements at TVC from 2015 – 2019 show that topographic drift sites accumulate deeper and more variable snow (mean ± stdev, 98 ± 70 cm) whereas tundra and open tundra sites are characterised by shallower, lower density snowpacks (38cm ± 16, 46 ± 12 cm) (Walker and Marsh, 2021). Shrub and tussock tundra dominate the TVC landscape, with tussock tundra covering approximately 37% of the study area and shrub tundra classes together accounting for nearly half of the landscape (Grünberg et al., 2020).

TVC has a comparatively rich dataset of meteorological and snow measurements, comprising near-continuous annual measurements of bulk snow density, snow depth and snow water equivalent (SWE) having been taken at TVC since 1991 at or around peak SWE (April-May) (Tutton et al., 2025). In addition, hourly gap-filled meteorological variables (1991 – 2023) were obtained from TVC's main meteorological station (Tutton et al., 2025). The combination of multi-decadal, near continuous meteorological and snow property measurements makes TVC well suited for training and evaluating a RF model for bulk snow density prediction. This study leveraged meteorological measurements from TVC used in conjunction with Arctic SVS2-Crocus (ASC, Woolley et al., 2025; Vionnet et al., 2025) bulk snow density simulations to train the RF model.

https://doi.org/10.5194/egusphere-2026-3363
Preprint. Discussion started: 20 July 2026

2.2 Random forest model development

The RF model was trained using bulk snow density data from six winter seasons (2001/02, 2006/07, 2007/08, 2012/13, 2014/15, 2016/17) simulated by ASC. These seasons, which span 1 Sep – 1 May, were selected based on the high agreement between ASC simulated density and depth to their associated snow course measurements, ensuring that the training framework was supplied with simulations underpinned by in-situ measurements. To identify these high-performing seasons, ASC-simulated and measured density–depth pairs from 29 available seasons (1991–2023) were analysed (Appendix B, 6.2). For each selected season, the ASC ensemble member (n=120) most closely matching the snow course measurement was chosen to represent the bulk snow density time-series for that season. The selected bulk snow density datapoints were then paired with corresponding measured meteorological variables, resulting in a training dataset of 1453 samples (6 snow seasons spanning 1 Sep – 1 May). The MATLAB RF regression function TreeBagger was used to build the RF model using a training:testing data split of 80:20. Cross-validation and hyperparameter tuning were performed using random partitioning (cvpartition), which may introduce temporal dependence leading to overestimation of model skill (Roberts et al., 2017), therefore, model performance was primarily assessed using an independent test period (2017 – 2023). The inclusion of additional seasons beyond the six selected yielded minimal improvement in RMSE supporting the chosen training configuration; the chosen density time series data were then paired with meteorological variables.

A set of meteorological features were used to train and test the RF model, and their relative importance for predicting bulk snow density was evaluated. The candidate meteorological features included shortwave radiation (SW, W m^{-2}), incoming longwave radiation (LW, W m^{-2}), snowfall rate (Sf, kg m^{-2} s^{-1}), rainfall rate (Rf, kg m^{-2} s^{-1}), air temperature (Ta, K), relative humidity (Rh, %), wind speed (Ua, m s^{-1}) and surface air pressure (Ps, Pa). For this study, only minimal feature engineering was undertaken, with two new input features being created: precipitation rate (pr, kg m^{-2} s^{-1}) calculated from combining Sf and Rf, and cumulative snowfall (mm) from the cumulative sum of Sf, converted to millimetres. Feature importance analysis was then applied to identify the combination of meteorological features resulting in the lowest model RMSE, resulting in the selection of SW, Sf, Ta and cumulative snowfall. Sf was retained despite a comparatively low importance score to test model sensitivity to snowfall patterns; particularly large snowfall events and the onset of the snow-covered season.

2.3 Future meteorological forcing data

The NA-CORDEX (North American Coordinated Regional Climate Downscaling Experiment) is a multi-model ensemble of dynamically downscaled regional climate projections covering North America, providing high-resolution meteorological forcing data under multiple RCP scenarios. The NA-CORDEX ensemble was bias adjusted to match the statistical characteristics of in-situ meteorological measurements from TVC (Tutton et al., 2025; Cannon, 2018; Cannon et al., 2022). The NA-CORDEX meteorological time series includes incoming shortwave and longwave radiation, precipitation, humidity, wind speed, air pressure, minimum and maximum air temperature and was generated from 33 GCM-RCM combinations under climate scenarios RCP 4.5 and 8.5. This bias-adjusted data was used to generate future projections of bulk snow density using the RF, and to drive future CLM5.0 simulations (2016 – 2100) as described in Rutherford et al. (2025). Since RF models are constrained by their training distribution, it was necessary to assess the distributional overlap between NA-CORDEX and the RF training data prior to generating future projections.

https://doi.org/10.5194/egusphere-2026-3363
Preprint. Discussion started: 20 July 2026

2.4 Uncertainty assessment

Predictions using RFs are most reliable in regions of predictor space that are well-sampled during training and become increasingly uncertain where the feature space differs considerably (Hateffard et al., 2024; Meyer and Pebesma, 2021). The Jensen Shannon Divergence (JSD) metric (Lin, 1991; Briët and Harremoës, 2009) was chosen to quantify divergence between the training meteorology and NA-CORDEX future meteorology. JSD (Equation 1) is a symmetrised and smoothed version of the Kullback-Leiber divergence (Joyce, 2011; Kullback, 1951) (Equation 2) and measures the similarity between two probability distributions (PDFs), in our case the RF training meteorology and NA-CORDEX projections. PDFs were generated using two-dimensional kernel density estimates for two of the most influential feature variables, cumulative snowfall and air temperature, and JSD calculated as follows:

$$\mathrm{JSD}(P \parallel Q) = \frac{1}{2}[D_{\mathrm{KL}}(P \parallel M) + D_{\mathrm{KL}}(Q \parallel M)] \quad (1)$$

$$D_{\mathrm{KL}}(P \parallel M) = \sum_i P_i \log_2\left(\frac{P_i}{M_i}\right) \quad (2)$$

where P and Q are the normalised PDFs of the training and projected meteorology, $M = \frac{1}{2}(P + Q)$ is their average distribution and D_{KL} denotes the Kullback-Leiber divergence. Higher JSD values indicate greater divergence between the two datasets (1 = perfect divergence), which suggests that a higher proportion of the NA-CORDEX data lie outside the bounds of the RF training data. Whereas lower JSD values indicate closer alignment between the two datasets (0 = perfect alignment) and suggest that the RF model is still operating within an interpolative regime. As a result, the JSD metric infers a degree of uncertainty for future predictions of bulk snow density where confidence in the model's predictive accuracy decreases the further that future meteorological conditions diverge from those in the training data.

2.5 Data insertion to CLM5.0

RF-derived snow bulk densities were inserted into CLM5.0 directly through the SoilThermProp subroutine of SoilTemperatureMod.F90 source file, part of the soil and snow temperature solver in the CLM5.0 timestep. In its default settings SoilThermProp calculates the snow bulk density (Equation 3) and snow thermal conductivity (Equation 4) (a full guide to variable symbols is shown in Table). In this study, the internally calculated bulk snow density was replaced with RF-derived bulk snow density.

$$\rho_{c,j} = \frac{m_{\mathrm{ice},c,j} + m_{\mathrm{liq},c,j}}{f_{\mathrm{sno}} \cdot \mathrm{d}z_{c,j}} \quad (3)$$

$$k_{c,j} = k_{\mathrm{air}} + (7.75 \times 10^{-5} \rho_{c,j} + 1.105 \times 10^{-6} {\rho_{c,j}}^2)(k_{\mathrm{ice}} - k_{\mathrm{air}}) \quad (4)$$

where c is the number of snow layers in column j, $\rho_{c,j}$ is bulk snow density computed from the fractions of ice m_{ice} and liquid m_{liq} components, snow layer thickness $\mathrm{d}z_{c,j}$ and the fraction of the ground covered by snow f_{sno}. The thermal conductivity of each snow layer $k_{c,j}$ is computed from $\rho_{c,j}$ and the thermal conductivities of ice (k_{ice}) and air (k_{air}) as per Jordan (1991). In addition to the default configuration of CLM5.0, two data insertion approaches were undertaken:

https://doi.org/10.5194/egusphere-2026-3363
Preprint. Discussion started: 20 July 2026

Table 1 - RF bulk snow density insertion methods to CLM5.0

Configuration name	**Description**
Default	Representing the standard CLM5.0 configuration with no changes to the SoilTemperatureMod
ρ^{ML}-derived K$_{eff}$	Replaces bulk snow density used in the default calculation of $k_{c,j}$ with bulk snow density derived from machine learning as follows: $k_{c,j} = k_{\mathrm{air}} + (7.75 \times 10^{-5}\rho_{\mathrm{ML}} + 1.105 \times 10^{-6}{\rho_{\mathrm{ML}}}^{2})(k_{\mathrm{ice}} - k_{\mathrm{air}})$ (5)
ρ^{ML}-derived K$_{eff}$ + snow layer scaling	Aims to maintain mass consistency in the snowpack by rescaling the modelled snow layers by the difference between default density and RF-density: $\mathrm{d}z_{c,j} = \mathrm{d}z_{c,j}\frac{\rho_{c,j}}{\rho_{\mathrm{ML}}}$ (6) This approach also independently replaced the state variable for bulk snow density: $\rho_{c,j} = \rho_{\mathrm{ML}}$ (7) which ensured that CLM5.0 snow physics routines outside of the K$_{eff}$ parameterisation accessed the RF-derived bulk density rather than the default.

The edited SoilTemperatureMod.F90, which included the RF-derived bulk snow densities, replaced the default source file before building the CLM5.0 model case. CLM5.0 error metrics for the conservation of mass in snow (ERRH2OSNO) and liquid water (ERRH2O) are consistently 1x10^{-15} mm or below across the three approaches – default, ρ^{ML}-derived K$_{eff}$ and ρ^{ML}-derived K$_{eff}$ + snow layer scaling – indicating that the modifications made do not disrupt the water mass balance in the model. The RF-CLM5.0 soil temperature simulations were validated against in-situ 10cm soil temperature measurements at TVC from Boike et al. (2023). Additionally, 2 m soil temperature measurements were obtained from an unpublished dataset using calibrated HOBO thermistor sensors (±0.25 °C accuracy; J. Boike, pers. comm., 2026).

2.6 CLM5.0 setup and parameter sensitivity

The CLM5.0 setup, except for changes to the SoilTemperatureMod.F90 is as described in Rutherford et al. (2025) and the same NA-CORDEX ensemble is used as driving meteorology. A range of parameter values for Ψ_{min}, Q_{10} and ch4q10 were used to capture physically plausible parameter variability as per Rutherford et al. (2025). The parameter range spanned an upper carbon response of -20 (Ψ_{min}), 1.5 (Q_{10}) and 1.33 (ch4q10) and a lower carbon response of -2 (Ψ_{min}) 7.5 (Q_{10}) and 4 (ch4q10). These combinations of Ψ_{min}, Q_{10} and ch4q10 are applied to each of the three approaches taken to represent bulk snow density and the associated thermal conductivity: 'default', 'ρ^{ML}-derived K$_{eff}$' and 'ρ^{ML}-derived K$_{eff}$ + snow layer scaling'. A resulting total of 198 experiments were undertaken, 66 for each of the three approaches and simulations performed over the 2016 – 2100 period to assess the impacts of each approach on future projections of soil temperature. Future CLM5.0 simulations focus on the winter season when snow is on the ground (i.e. the snow-covered non-growing season) and we define this period as the time when all CLM5.0 ensemble members (RCP 4.5 n=6, RCP 8.5 n=27) agree that SWE is > 5 mm as outlined by Krinner et al. (2018), filtering bulk snow density and soil temperature simulations by these constraints.

https://doi.org/10.5194/egusphere-2026-3363
Preprint. Discussion started: 20 July 2026

3 Results

3.1 Performance of the random forest bulk snow density model

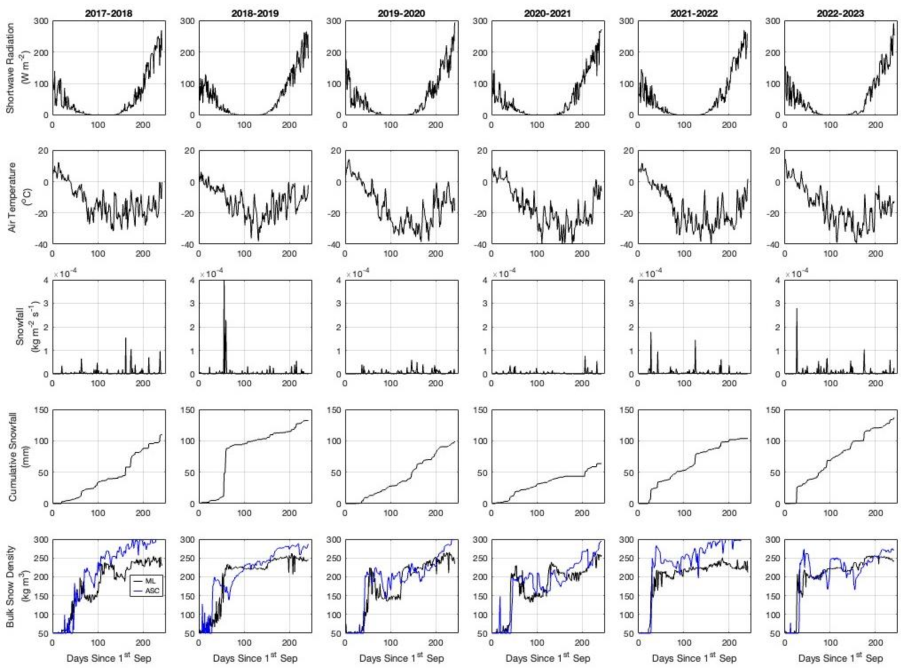

Figure 1 - Meteorological inputs and validation plots for prediction of bulk snow density from meteorology using a random forest regression model over 6 winter seasons 2017 – 2023 (September – 1 May. Rows 1 – 4 show the measured meteorological data features for each year which include shortwave radiation (SW, W m^{-2}), air temperature (Ta, K), snowfall rate (Sf, kg m^{-2} s^{-1}), and cumulative snowfall (mm). Row 5 shows bulk snow density predictions from the random forest model (black) compared against ASC bulk snow density ensemble mean (n=120) (blue).

RF predictions tended to underestimate ASC simulated snow density with an average difference of 59 kg m^{-3} by the end of the snow season (nominally 1 May) (Figure 1). Six years of measured meteorological data for winter seasons 1 September to 1 May 2017 – 2023 were used to test the RF model and assess conformity of RF predictions to ASC simulations (Figure 1). The timing and rate of bulk snow density increase at the start of snow accumulation in RF predictions aligns well with ASC simulations, except in 2018/19 where ASC simulations show a rapid increase in bulk snow density to 195 kg m^{-3} which can be attributed to a small snowfall event ~50 days since 1st September. Both RF and ASC show low bulk snow density (0 – 100 kg m^{-3}) soon after snow onset (day 0 – 50) which rapidly increased during accumulation before stabilising later in the season (day 100 – 250) around 250 – 300 kg m^{-3}. The RF model simulates ASC bulk snow density with an average MAE of 32 kg m^{-3} across the 2017 – 2023 winter seasons, with the best predictive ability occurring during early accumulation. The timing of bulk snow density increases in the RF predictions were strongly dependent on accumulation of snowfall and this is reflected in its feature importance score which is the highest of all chosen features.

https://doi.org/10.5194/egusphere-2026-3363
Preprint. Discussion started: 20 July 2026

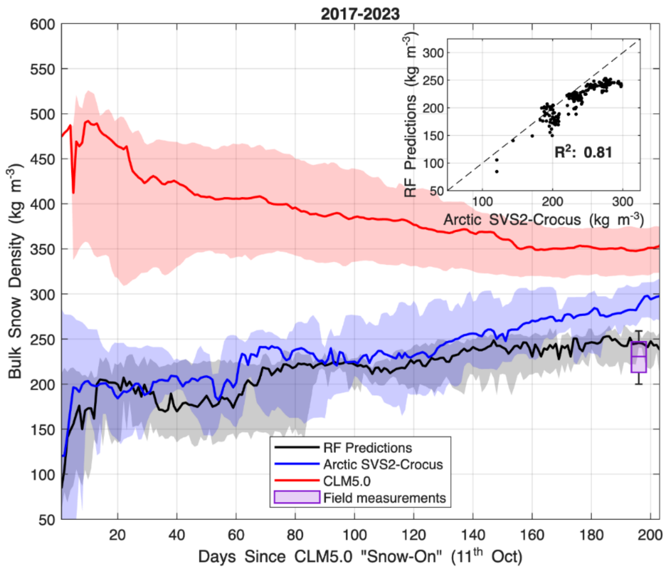

Figure 2 – Median bulk snow density over winter seasons 2017–2023 from RF predictions (black), ASC (blue), and CLM5.0 (red). ASC and CLM5.0 lines represent the ensemble mean (n = 120, n = 33) with the 2017–2023 seasonal median shown. Shaded regions show the interannual minimum–maximum range across the six seasons. The purple boxplot shows measured annual mean bulk snow densities from field campaigns at Trail Valley Creek (n = 5, 23 March – 24 April, no campaign in 2019/20). The x-axis origin corresponds to the earliest CLM5.0 ensemble mean snow-on date (11 October), with all years contributing data from day 0 onwards; the period shown reflects consistent snow-on conditions across all ensemble members (SWE > 5 mm). Inset: RF predictions versus ASC daily bulk snow density (2017 – 2023).

RF predictions were then compared to density measurements taken around the timing of peak SWE (23 March – 24 April) for five snow seasons between 2017 – 2023 (no campaign in 2019/20). Median RF predictions of bulk snow density (245 kg m^{-3}) were closer to field measurements (230 kg m^{-3}) than ASC (287 kg m^{-3}) and default CLM5.0 simulations (348 kg m^{-3}). The RF model generally predicted lower bulk snow densities than both ASC and CLM5.0 throughout the winter. Median RF values were, on average, 21 kg m^{-3} lower than ASC simulations and 175 kg m^{-3} lower than CLM5.0 simulations (Figure 2). Overall, the RF model reproduced both the magnitude and seasonal evolution of ASC bulk snow density, outperforming CLM5.0. However, RF predictions diverged from ASC simulations at 150 days post snow onset with the average difference increasing from 15 kg m^{-3} (day 1 – 150) to 34 kg m^{-3} (day 150 – 204).

https://doi.org/10.5194/egusphere-2026-3363
Preprint. Discussion started: 20 July 2026

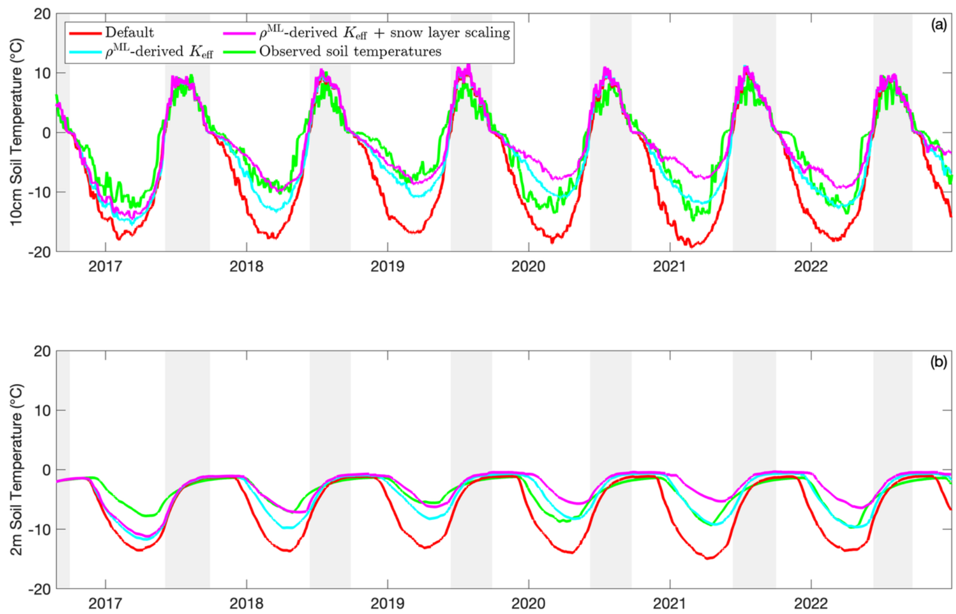

Figure 3 - Time series of 10 cm and 2 m median soil temperature driven by an ensemble of NA-CORDEX meteorologies (2016 – 2023) under RCP 4.5 (a, n = 6) and RCP 8.5 (b, n = 27). Default CLM5.0 (red) is compared with two bulk snow density data insertion approaches: ρ^{ML}-derived K_{eff} (cyan) and ρ^{ML}-derived K_{eff} + snow layer scaling (magenta), evaluated against in-situ soil temperature measurements (green) at TVC from Boike et al. (2023). Grey shading indicates the snow-free period.

Simulated soil temperatures were evaluated against field measurements during winter (SWE > 5 mm) and ρ^{ML} approaches improved RMSE by approximately 2 – 3 °C (2016 – 2023) at both depths (10 cm and 2 m); ρ^{ML}-derived K_{eff} approach provided the best overall agreement with the observations (Figure 3). Default CLM5.0 exhibited a persistent cold bias at 10 cm, with median winter soil temperatures of −10.5°C versus −5.8°C observed (bias = −4.7°C). Both ρ^{ML} approaches substantially reduced this bias: ρ^{ML}-derived K_{eff} yielded −6.6°C (bias = –0.8) and ρ^{ML} -derived K_{eff} + snow layer scaling −4.4°C (+1.4°C).

The cold bias propagated to 2 m (default: −9.3°C; observed: −4.0°C; bias = −5.3°C), where ρ^{ML} -derived K_{eff} and ρ^{ML} -derived K_{eff} + snow layer scaling again reduced the bias, yielding −4.7°C (–0.7°C) and −2.7°C (+1.3°C) respectively. The snow layer scaling approach increased mean snow depth by ~10 cm (2017–2023) causing a warm overestimation in winter soil temperatures relative to observations. All configurations also lagged spring soil warming, with observed 10 cm temperatures reaching 0°C approximately 10–24 days earlier than simulated values in four of six winters.

https://doi.org/10.5194/egusphere-2026-3363
Preprint. Discussion started: 20 July 2026

3.2 RF training data vs NA-CORDEX meteorology

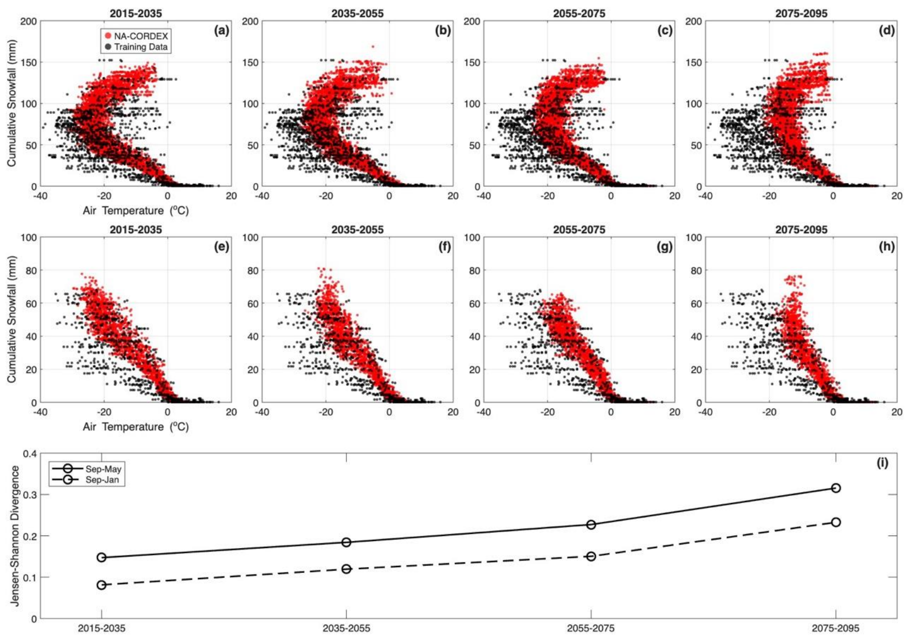

Figure 4 - Random forest training data (black dots) versus future NA-CORDEX (red dots) for air temperature and cumulative snowfall in 20-year time windows 2015-2095 for 1 September to 1 May (a – d) and 1 September to 1 January (e – h). Panel (i) is a quantification the difference in probability distribution between training and NA-CORDEX datasets using Jensen-Shannon Divergence (JSD, 'o'), 0 indicates perfect alignment and 1 indicates perfect divergence.

Analysis of the divergence between the training and NA-CORDEX meteorological datasets indicates a decrease in confidence with increasing projection timescale. NA-CORDEX projections show that average daily winter air temperatures increase from -13 to -7 °C between 2015 and the end of the century, whereas average accumulated snowfall remains similar (59 – 62 mm). Early winter season (1 Sep – 1 Jan) training data exhibited greater distributional similarity to NA-CORDEX than full season data (1 Sep – 1 May) by an average JSD value of 0.07 (2015 – 2095). JSD increased from 2015 onwards at a rate of 0.0018 yr^{-1} (1 Sep – 1 Jan) – 0.0021 yr^{-1} (1 Sep – 1 May). Relative to the 2015 – 2035 baseline, JSD increased by approximately 110% (1 Sep – 1 Jan) and 190 % (1 Sep – 1 May) by 2095 in the full and late season timescales, indicating a distributional shift and a reduction in the representativeness of the RF training data under future climate conditions.

https://doi.org/10.5194/egusphere-2026-3363
Preprint. Discussion started: 20 July 2026

3.3 Future bulk snow density predictions and comparison with CLM5.0

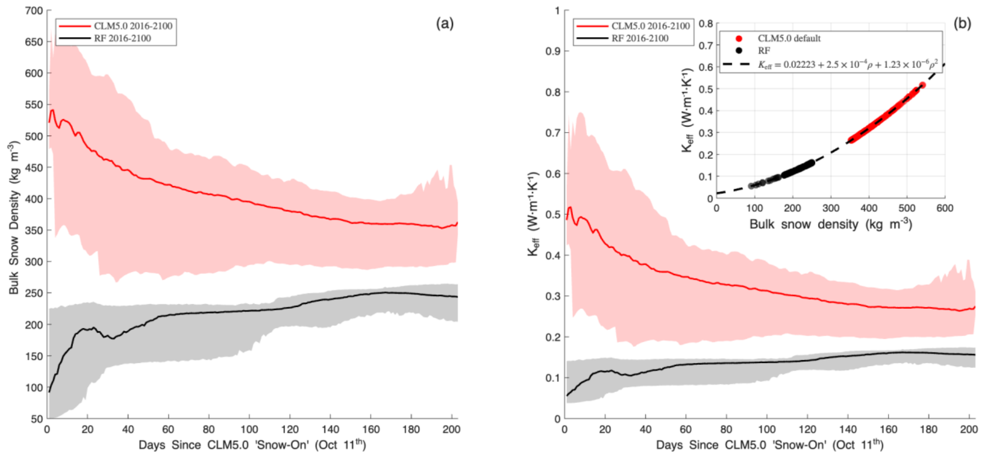

Figure 5 – Median bulk snow density (a) and K_{eff} (b) across the 2016 – 2100 period for RF-predicted (black) and default CLM5.0 (red), derived from the NA-CORDEX ensemble mean. Shaded areas represent inter-annual range across 2016 – 2100. The inset shows the relationship between bulk snow density and K_{eff} following Jordan (1991), with default CLM5.0 (red) and RF-predicted density superimposed. The x-axis is referenced to the earliest CLM5.0 ensemble mean snow-on-date (Oct 11th) with all years contributing data from day 0 onwards.

Winter season RF predictions (2016 – 2100) showed gradual increases in bulk snow density over time, stabilising at ~200 – 250 kg m^{-3}, which is consistent with seasonal TVC field measurements (average 236 kg m^{-3}, 1991 – 2023) (Figure 5). Median RF predicted bulk snow densities were up to 450 kg m^{-3} lower than CLM5.0 simulated bulk snow densities from 2016 – 2100, with the difference reducing to approximately 100 kg m^{-3} by the end of the season. CLM5.0 simulations also displayed a higher variability, with a range of 266 – 674 kg m^{-3} compared with a range of 50 – 265 kg m^{-3} for RF predictions. Both RF and CLM5.0 show a reduction in variability beyond ~50 days post snow-on, however, RF predictions plateau in the upper bound in contrast to the broader range exhibited by CLM5.0. CLM5.0 produced unrealistically high snow densities at the start of the winter season (~350 – 650 kg m^{-3}), exceeding values typical of established wind slab layering (~350 – 450 kg m^{-3}). As a consequence of the lower snow densities, K_{eff} resulting from RF snow densities was 0.19 W m^{-1} K^{-1} lower on average than default CLM5.0, by contrast CLM5.0 snowpacks maintained high K_{eff} (> 0.3 W m^{-1} K^{-1}).

https://doi.org/10.5194/egusphere-2026-3363
Preprint. Discussion started: 20 July 2026

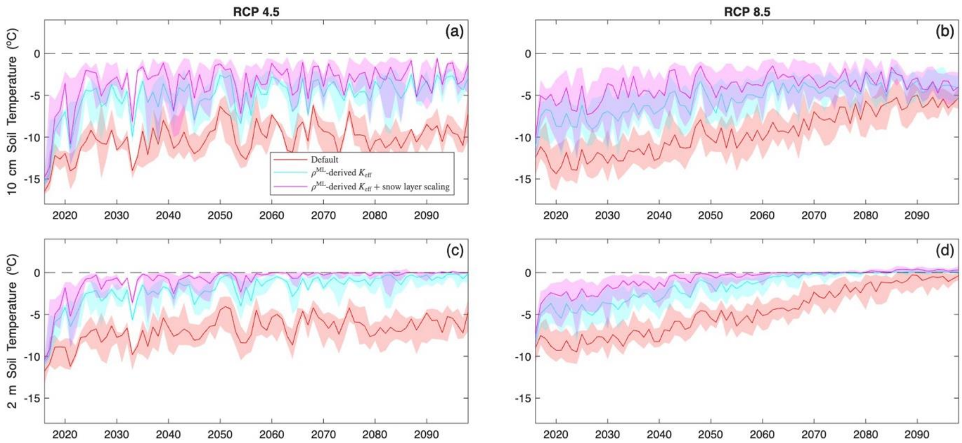

Figure 6 - Future CLM5.0 projections of median winter 10 cm and 2 m soil temperature driven by an ensemble of NA-CORDEX meteorologies (2016 – 2100) under RCP 4.5 (a, c, n = 6) and RCP 8.5 (b, d, n = 27). Default CLM5.0 (red) is compared with CLM5.0 driven by RF predicted snow densities under two approaches ρ^{ML}-derived K_{eff} (cyan) and ρ^{ML}-derived K_{eff} + snow layer scaling (magenta). The shaded areas reflect uncertainty due to both climate forcing (NA-CORDEX) and model parameter sensitivity Ψ_{min}, Q_{10} and $Q_{10}CH_4$.

Direct insertion of RF-predicted snow densities into CLM5.0 consistently raised simulated winter soil temperatures by approximately 5 – 7 °C at 10 cm depth under RCP4.5 and 4 – 5 °C under RCP8.5 from 2016 – 2100, compared to default CLM5.0 (Figure 6, a, b). Across both RCP scenarios, the ρ^{ML}-derived K_{eff} + snow layer scaling approach consistently produced the warmest soil temperatures (2016 – 2100 mean: -3.5 to -4.0 °C), followed by the ρ^{ML}-derived K_{eff} approach (-5.0 to -5.3 °C), while the default configuration remained substantially colder (-9 to -10 °C). This thermal offset propagated to 2 m depth, where ρ^{ML} approaches simulated mean winter soil temperatures of -2 to -0.7 °C compared with -6 to -4 °C under the default, with 2 m temperatures under RCP 8.5 reaching 0 °C by approximately 2080 – 2100, a threshold not approached under the default CLM5.0 configuration.

Initial soil temperatures in 2016 were 4 – 5 °C lower under RCP4.5 than RCP8.5 across all configurations, and between 2016 – 2100 interannual variability was greater under RCP4.5 (median ± 15 °C) than under RCP8.5 (median ± 10 °C). Default CLM5.0 diverges from the two ρ^{ML} approaches in both magnitude and trajectory. Default CLM5.0 begins with a colder baseline temperature but warms at a faster rate, whereas ρ^{ML} approaches begin warmer but warm more slowly. For example, under RCP8.5, linear fits over 2016 – 2100 indicate a more rapid increase in winter soil temperatures in CLM5.0 default (0.1 °C yr^{-1}) than either of the two ρ^{ML} approaches (0.06 °C yr^{-1} and 0.03 °C yr^{-1}). In contrast to the default run, soil temperatures under both ρ^{ML} approaches increased from their baseline temperature until approximately 2060 where they stabilised at -4 to -5 °C through 2100. Soil temperature differences between the two ρ^{ML} approaches under RCP8.5 persisted until ~2080, after which soil temperatures converged.

https://doi.org/10.5194/egusphere-2026-3363
Preprint. Discussion started: 20 July 2026

4 Discussion

4.1 Random forest model development

The performance of the RF model suggests that it can successfully emulate Arctic tundra bulk snow density evolution as represented by ASC, establishing it as a viable tool for integration into a process-based model such as CLM5.0. The RF model achieves an RMSE of 32 kg m^{-3} across six validation years, which falls within reported measurement errors of ± 20 – 40 kg m^{-3} for traditional volumetric sampling of tundra snow density (Conger and McClung, 2009; Proksch et al., 2016). Evaluation of RF model performance on six winters of unseen meteorology suggests an RF model can generalise well the complex seasonally non-linear relationships linking meteorological features to tundra bulk snow density. Although itself not physically based, the RF model shows a strong ability to reproduce seasonal bulk snow density learned from physically based ASC simulations. In particular, the RF model captures the gradual increase in bulk snow density over time during early winter (Sturm et al., 1995) and avoids unrealistically high densities seen in CLM5.0 outputs which are not physically consistent with observed snowpack evolution (Zhao et al., 2023; Che et al., 2025). Instead, the RF model reproduces slower densification trajectories seen in ASC simulations and stabilises around ~200 – 250 kg m^{-3}, which is consistent with field measurements. This performance stems from ASC simulations which better represent tundra snowpack bulk density compared to the default version of SVS2-Crocus but critically does not explicitly simulate vapour transport processes responsible for depth hoar. These vapour transport processes remain highly uncertain in snow and earth system modelling due to the complexity of representing them numerically (Brondex et al., 2023; Domine et al., 2019; Woolley et al., 2024). While the RF performs well compared to CLM5.0, it fundamentally inherits limitations inherent of ASC.

Divergence between the RF training dataset and the NA-CORDEX ensemble highlights a key limitation of default RF algorithms: the inability to predict outside of the training range (Kanda and Fletcher, 2025). Standard RFs are constrained by piecewise constant predictions which reduce the reliability of future bulk snow density predictions under climate conditions not represented in the training data. While the JSD analysis indicates an increasing shift between training and testing domain, it does not fully characterise the specific combinations of predictor features. Further work could investigate multivariate similarity metrics to better constrain model performance on uncertain climate conditions. Additionally, hybrid model-based variants such as mobForest (Garge et al., 2013) fit linear models within leaf nodes which allow predictions to follow local trends rather than being anchored to the mean of training samples within each leaf. Such approaches could be used to improve the robustness of RF-based bulk snow density projections under novel future conditions.

Despite divergence in training vs NA-CORDEX, the JSD analysis shows confidence in future RF predictions is highest in the early winter (1 Sep – 1 Jan), a period where snow has an important influence on soil temperatures (Rixen et al., 2022) and subsequent soil carbon emissions (Mavrovic et al., 2023; Rutherford et al., 2025; Schimel et al., 2006). Early winter is a critical period for soil carbon release as, during the early freeze-up and zero-curtain periods, soils remain relatively warm and moist, creating favourable conditions for release of CH_4 (Zona et al., 2016; Mastepanov et al., 2013) and CO_2 (Natali et al., 2019). Default parameterisations of CLM5.0 produces overly dense snow, particularly in this early winter period, which exacerbate cold soil temperature bias compared with later in the winter. Underestimation of early winter respiration is a known limitation of ESMs (Commane et al., 2017), and overestimation of snow density by the default configuration of CLM5.0 likely contributes to

https://doi.org/10.5194/egusphere-2026-3363
Preprint. Discussion started: 20 July 2026

supressed soil temperatures and carbon fluxes in this period. By contrast, the RF predictions more realistically represent bulk snow density in early winter, improving simulation of snowpack evolution and therefore regulation of soil–atmosphere carbon exchange.

RF bulk snow density predictions are consistently lower than those simulated by CLM5.0 and more closely aligned to late winter field measurements, making them a more appropriate estimation of bulk snow density evolution in contemporary tundra environments. Improvements to the default CLM5.0 snow module, particularly a new wind-dependent fresh snow density function from van Kampenhout et al. (2017) with the primary aim of better simulating snow density over ice sheets, has unintentionally increased bulk snow density over most of the Arctic tundra compared to CLM4.5 (Lawrence et al., 2019; Damseaux et al., 2024). As snow density is intrinsically linked to K_{eff} (Calonne et al., 2011), unrealistically high densities exaggerate heat transfer through Arctic snowpacks to the underlying soil. Dutch et al. (2024) estimated that CLM5.0 overestimates K_{eff} in tundra by a factor of 3 in tundra conditions, while in this study, differences between RF K_{eff} predictions and CLM5.0 K_{eff} reach up to a factor of 5. Such overestimates of K_{eff} indicate that the default parameterisation of CLM5.0 simulates K_{eff} indicative of harder, denser snow such as wind slab, whereas Sturm et al. (1995) highlighted notable influence of low density snow types such as depth hoar on K_{eff} in tundra snow. Consequently, the RF predicts bulk snow density and K_{eff} values that are more representative of tundra snowpack conditions. Overall, the RF model provides more realistic estimates of tundra bulk snow density than the default configuration of CLM5.0 and demonstrates potential for reducing cold soil biases in future projections of soil temperature.

Despite the improvements in bulk snow density offered by the RF model, a key limitation is its training on a single site, meaning its transferability to different Arctic sites and local meteorological conditions remains uncertain. While the longer-term goal is a pan-Arctic parameterisation for snow density; this paper represents a proof of concept at a single site, and future work should aim to extend the framework to additional sites to develop a more spatially explicit model. Candidate sites for extending the spatial capabilities of the model could include but are not limited to Imnavait Creek and Upper Kuparuk, Alaska (Stuefer et al., 2020), Sodankyla, Finland (Essery et al., 2016), Bylot island, Canada (Domine et al., 2021), Cambridge Bay, Canada (Levasseur et al., 2021) which have rich history of snow and meteorological measurements, and span a range of tundra snow climate regimes.

4.2 Insertion of RF bulk snow density to CLM5.0

Our integration to CLM5.0 aligns with growing evidence that hybrid modelling, combining machine learning with physically based models, outperforms standalone models when applied to snow related variables (Zhao et al., 2026). Recent studies have demonstrated the potential of hybrid modelling frameworks that integrate physically-based snow models with machine learning to improve prediction accuracy. For example, Pomarol Moya et al. (2026) combined outputs from the Crocus snow model with machine learning algorithms and found that RF outperformed neural network and long short term memory methods in applications with limited observational data. Resulting from our integration of RF bulk density to CLM5.0, we recommend the ρ^{ML}-derived K_{eff} approach for reducing soil temperature RMSE and inherent soil temperature bias in default CLM5.0 winter soil temperature simulations. The ρ^{ML}-derived K_{eff} + snow layer scaling approach is a useful sensitivity test of physically consistent snowpack adjustments but is not recommended as the rescaling deepens the snowpack, increasing its insulative capacity (Slater et al., 2017; Schimel et al., 2004) and soils become overly warm relative to observations. Results suggest that improving snow thermal properties alone can improve model performance, however, achieving fully

https://doi.org/10.5194/egusphere-2026-3363
Preprint. Discussion started: 20 July 2026

consistent snowpack representation will require a more integrated treatment of snow structure and evolution within CLM5.0.

Default CLM5.0 captures summer soil temperatures well but exhibits cold biases in winter, misrepresenting key freeze-thaw dynamics and the winter impact on overall Arctic carbon budgets (Natali et al., 2019). Default CLM5.0 underrepresents delayed freeze-up in early winter, whereas the ρ^{ML} approaches are consistent with a more realistic representation of early winter freeze-up dynamics. This is key, as early winter soil temperatures exert a strong control over the timing and magnitude of wintertime carbon emissions (Fahnestock et al., 1999; Zona et al., 2016). Further, a slower-than-observed increase in soil temperature during the melt period suggests simulations underestimates the efficiency of energy transfer associated with snowmelt, particularly delivery of meltwater to the snow–soil interface and associated latent heat release, which typically drives rapid soil warming (Zhao et al., 2022). Energy exchanges during water phase changes also help explain the observable plateau in projected near surface soil temperature towards the end of the century, where, as an increasing proportion of the soil column approaches 0 °C the latent heat of fusion required for thaw absorbs incoming energy, producing a thermal buffering effect that limits further warming (Romanovsky and Osterkamp, 2000).

4.3 Future projections and implications for soil temperature, permafrost and carbon release

Future projections (2016 – 2100) show that snow cover persists throughout the 21st century and its representation exerts a strong control on simulated soil temperatures. The ρ^{ML} approaches consistently elevate soil temperatures under RCP4.5 and 8.5 compared to default CLM5.0 bulk snow density parametrisations, highlighting that snow density parameterisation is crucial for soil temperature projections. Sensitivity to simulated bulk snow density is particularly pronounced under RCP8.5 which shows a clear upward trend in soil temperatures in contrast with more stable temperatures under RCP4.5. Divergence between RCP 4.5 and 8.5 suggests that uncertainties in snow density parameterisation become increasingly consequential under increased climate warming, where small changes determine whether soils remain frozen or approach thaw. By reducing biases in snow representation, the ρ^{ML} approaches mitigate errors which propagate to soil temperature (Slater et al., 2017) and carbon flux simulations (Dutch et al., 2024; Rutherford et al., 2025).

Accurate simulation of snow–soil interactions requires not only improved parameterisations of snow thermal conductivity but also realistic representation of bulk snow density and depth as first-order controls on winter soil temperatures. Given the temperature sensitivity of microbial decomposition near 0 °C (Schuur et al., 2015; Natali et al., 2019), elevated winter soil temperatures under future warming scenarios have capacity to drive increased carbon emissions, with simulated soil temperatures at 2 m depth indicating thaw of previously frozen soil by 2080 under RCP8.5. Prior assessments using default CLM configurations have projected losses of northern permafrost soil carbon under RCP8.5 by 2100 (McGuire et al., 2018), but these estimates likely represent a conservative lower bound, as default CLM5.0 and earlier versions do not accurately represent Arctic bulk snow density and its thermal influence on soil temperatures (Damseaux et al., 2024). The RF-derived parameterisation presented here directly addresses this source of uncertainty.

https://doi.org/10.5194/egusphere-2026-3363
Preprint. Discussion started: 20 July 2026

5 Conclusions

The RF model reproduces the seasonal evolution of bulk snow density simulated by the Arctic SVS2-Crocus model and aligns closely with field measurements collected around peak SWE between 2017 and 2023. RF performance (MAE = 32 kg m^{-3}) was within the error of traditional tundra snow density measurements when tested on the 2017 – 2023 period. Application of RF-derived snow densities decreased CLM5.0 soil temperature RMSE at 10 cm and 2 m depth by approximately 2 – 3 °C relative to field measurements (2017 – 2023). When applied to future meteorological projections, RF-predicted snow densities were up to five times lower than those simulated by the default CLM5.0 configuration, indicating a substantial influence on snow thermal conductivity and, consequently, soil temperature. Future CLM5.0 projections (2016 – 2100) indicated that snow density parameterisation exerts a first-order control on simulated soil temperatures, with RF-derived densities consistently elevating winter soil temperatures relative to default CLM5.0 under both RCP4.5 and 8.5. Consequently, future simulations of permafrost thaw that do not accurately capture snow bulk density and associated thermal properties likely produce conservative estimates of permafrost carbon release. Integration of RF-derived snow densities into CLM5.0 represents a promising pathway for reducing cold-soil biases and improving the realism of soil temperature projections under future climate scenarios. Further work should prioritise expanding the RF training dataset with in-situ observations and evaluating the RF model across broader climatic conditions and Arctic sites.

https://doi.org/10.5194/egusphere-2026-3363
Preprint. Discussion started: 20 July 2026

6 Appendices

6.1 Appendix A

CLM5.0 simulations (2016 – 2023) yielded 10 cm soil temperature RMSE of 5.9 °C (default), 3.0 °C (ρ^{ML}-derived K_{eff}) and 3.9 °C (ρ^{ML}-derived K_{eff} + snow layer scaling) relative to observations (Figure 3). At 2 m depth, soil temperatures exhibited an RSME of 4.5 °C (default), 1.8 °C (ρ^{ML}-derived K_{eff}) and 2.2 °C (ρ^{ML}-derived K_{eff} + snow layer scaling).

6.2 Appendix B – training years selection

The differences between ASC ensemble member and the associated field measurement were normalised by the maximum absolute difference observed across all years for each variable (snow density and snow depth), yielding a relative performance score between 0 and 1. The selected years exhibited performance scores between 0.08 and 0.29, placing them among the best-performing seasons within the full 1991 – 2023 dataset (range: 0.06–0.76).

6.3 Appendix C

Table C1 - Variables included in the calculation of snow bulk density and snow thermal conductivity in CLM5.0 with their equation symbol matched to the corresponding Fortran variable as per model source code.

Fortran variable	Symbol	Units	Description
bw(c,j)	$\rho_{c,j}$	kg m^{-3}	Snow layer bulk density
h2osoi_ice(c,j)	$m_{ice,c,j}$	kg m^{-2}	Layer ice mass per unit area
h2osoi_liq(c,j)	$m_{liq,c,j}$	kg m^{-2}	Layer liquid mass per unit area
dz(c,j)	$dz_{c,j}$	m	Layer thickness
frac_sno(c)	f_{sno}	–	Snow cover fraction
thk(c,j)	$k_{c,j}$	W m^{-1} K^{-1}	Snow layer thermal conductivity
tkair, tkice	k_{ice} k_{air}	W m^{-1} K^{-1}	Conductivities of air and ice

https://doi.org/10.5194/egusphere-2026-3363
Preprint. Discussion started: 20 July 2026

7 Code and data availability

Code and data required to produce figures is available at https://doi.org/10.5281/zenodo.20558314. The NA-CORDEX climate projections are available at https://doi.org/10.5281/zenodo.17112930.

8 Author Contributions

Experimental Design, CORDEX Bias Correction, CLM5.0 and ASC Simulations, Analysis and Draft preparation; JR, NR, LW, AC, GW, JB. Field measurements; JB. Supervision; NR, LW. All authors were involved in reviewing and editing prior to submission.

9 Competing Interests

The authors declare no competing interests.

10 Acknowledgements

JR was funded by a Research and Development Fund (RDF) Studentship from Northumbria University. The work was supported by a National Environmental Research Council (NERC) Seedcorn grant awarded to NR and LW; Carbon Emissions Under Arctic Snow (CEAS) project reference: NE/W003686/1.

11 References

Bigalke, S. and Walsh, J. E.: Future changes of snow in Alaska and the Arctic under stabilized global warming scenarios, Atmosphere, 13, 541, https://doi.org/10.3390/atmos13040541, 2022.

Boike, J., Miesner, F., Bornemann, N., Cable, W. L., and Grünberg, I.: Trail Valley Creek, NWT, Canada Soil Moisture and Temperature 2016 et seq, https://doi.org/10.1594/PANGAEA.962726, 2023.

Bouvet, L., Calonne, N., Flin, F., and Geindreau, C.: Heterogeneous grain growth and vertical mass transfer within a snow layer under a temperature gradient, The Cryosphere, 17, 3553-3573, https://doi.org/10.5194/tc-17-3553-2023, 2023.

Breiman, L.: Random forests, Machine learning, 45, 5-32, 2001.

Briët, J. and Harremoës, P.: Properties of classical and quantum Jensen-Shannon divergence, Physical Review A—Atomic, Molecular, and Optical Physics, 79, 052311, https://doi.org/10.1103/PhysRevA.79.052311, 2009.

Brondex, J., Fourteau, K., Dumont, M., Hagenmuller, P., Calonne, N., Tuzet, F., and Löwe, H.: A finite-element framework to explore the numerical solution of the coupled problem of heat conduction, water vapor diffusion, and settlement in dry snow (IvoriFEM v0. 1.0), Geoscientific Model Development, 16, 7075-7106, https://doi.org/10.5194/gmd-16-7075-2023, 2023.

Calonne, N., Flin, F., Morin, S., Lesaffre, B., du Roscoat, S. R., and Geindreau, C.: Numerical and experimental investigations of the effective thermal conductivity of snow, Geophysical research letters, 38, https://doi.org/10.1029/2011GL049234, 2011.

Cannon, A. J.: Multivariate quantile mapping bias correction: an N-dimensional probability density function transform for climate model simulations of multiple variables, Climate dynamics, 50, 31-49, https://doi.org/10.1007/s00382-017-3580-6, 2018.

Cannon, A. J., Alford, H., Shrestha, R. R., Kirchmeier-Young, M. C., and Najafi, M. R.: Canadian Large Ensembles Adjusted Dataset version 1 (CanLEADv1): Multivariate bias-corrected climate model outputs for terrestrial modelling and attribution studies in North America, https://doi.org/10.1002/gdj3.142, 2022.

Che, T., Dai, L., and Li, X.: Spatiotemporal distribution of seasonal snow density in the Northern Hemisphere based on in situ observation, Research in Cold and Arid Regions, https://doi.org/10.1016/j.rcar.2025.02.004, 2025.

Christensen, J. H., Kanikicharla, K. K., Aldrian, E., An, S. I., Cavalcanti, I. F. A., de Castro, M., Dong, W., Goswami, P., Hall, A., and Kanyanga, J. K.: Climate phenomena and their relevance for future regional climate change, in: Climate change 2013 the physical science basis: Working group I contribution to the fifth assessment report of the intergovernmental panel on climate change, Cambridge University Press, 1217-1308, https://doi.org/10.1017/CBO9781107415324.028, 2013.

Cohen, J., Ye, H., and Jones, J.: Trends and variability in rain-on-snow events, Geophysical Research Letters, 42, 7115-7122, https://doi.org/10.1002/2015GL065320, 2015.

Commane, R., Lindaas, J., Benmergui, J., Luus, K. A., Chang, R. Y.-W., Daube, B. C., Euskirchen, E. S., Henderson, J. M., Karion, A., and Miller, J. B.: Carbon dioxide sources from Alaska driven by increasing early winter respiration from Arctic tundra, Proceedings of the National Academy of Sciences, 114, 5361-5366, https://doi.org/10.1073/pnas.1618567114, 2017.

Conger, S. M. and McClung, D. M.: Comparison of density cutters for snow profile observations, Journal of Glaciology, 55, 163-169, https://doi.org/10.3189/002214309788609038, 2009.

Damseaux, A., Matthes, H., Dutch, V. R., Wake, L., and Rutter, N.: Impact of Snow Thermal Conductivity Schemes on pan-Arctic Permafrost Dynamics in CLM5. 0, EGUsphere, 2024, 1-29, https://doi.org/10.5194/tc-19-1539-2025, 2024.

Derksen, C., Lemmetyinen, J., Toose, P., Silis, A., Pulliainen, J., and Sturm, M.: Physical properties of Arctic versus subarctic snow: Implications for high latitude passive microwave snow water equivalent retrievals, Journal of Geophysical Research: Atmospheres, 119, 7254-7270, https://doi.org/10.1002/2013JD021264, 2014.

Derksen, C., Silis, A., Sturm, M., Holmgren, J., Liston, G. E., Huntington, H., and Solie, D.: Northwest Territories and Nunavut snow characteristics from a subarctic traverse: Implications for passive microwave remote sensing, Journal of Hydrometeorology, 10, 448-463, https://doi.org/10.1175/2008JHM1074.1, 2009.

Domine, F., Barrere, M., Sarrazin, D., Morin, S., and Arnaud, L.: Automatic monitoring of the effective thermal conductivity of snow in a low-Arctic shrub tundra, The cryosphere, 9, 1265-1276, https://doi.org/10.5194/tc-9-1265-2015, 2015.

Domine, F., Lackner, G., Sarrazin, D., Poirier, M., and Belke-Brea, M.: Meteorological, snow and soil data (2013–2019) from a herb tundra permafrost site at Bylot Island, Canadian high Arctic, for driving and testing snow and land surface models, Earth System Science Data, 13, 4331-4348, https://doi.org/10.5194/essd-13-4331-2021, 2021.

Domine, F., Belke-Brea, M., Sarrazin, D., Arnaud, L., Barrere, M., and Poirier, M.: Soil moisture, wind speed and depth hoar formation in the Arctic snowpack, Journal of Glaciology, 64, 990-1002, https://doi.org/10.1017/jog.2018.89, 2018.

Domine, F., Picard, G., Morin, S., Barrere, M., Madore, J. B., and Langlois, A.: Major issues in simulating some Arctic snowpack properties using current detailed snow physics models: Consequences for the thermal regime and water budget of permafrost, Journal of Advances in Modeling Earth Systems, 11, 34-44, https://doi.org/10.1029/2018MS001445, 2019.

Dutch, V. R., Rutter, N., Wake, L., Sandells, M., Derksen, C., Walker, B., Hould Gosselin, G., Sonnentag, O., Essery, R., and Kelly, R.: Impact of measured and simulated tundra snowpack properties on heat transfer, The Cryosphere, 16, 4201-4222, https://doi.org/10.5194/tc-16-4201-2022, 2022.

Dutch, V. R., Rutter, N., Wake, L., Sonnentag, O., Hould Gosselin, G., Sandells, M., Derksen, C., Walker, B., Meyer, G., and Essery, R.: Simulating net ecosystem exchange under seasonal snow cover at an Arctic tundra site, Biogeosciences, 21, 825-841, https://doi.org/10.5194/bg-21-825-2024, 2024.

Essery, R., Kontu, A., Lemmetyinen, J., Dumont, M., and Ménard, C. B.: A 7-year dataset for driving and evaluating snow models at an Arctic site (Sodankylä, Finland), Geoscientific Instrumentation, Methods and Data Systems, 5, 219-227, https://doi.org/10.5194/gi-5-219-2016, 2016.

Fahnestock, J. T., Jones, M. H., and Welker, J. M.: Wintertime CO2 efflux from arctic soils: implications for annual carbon budgets, Global Biogeochemical Cycles, 13, 775-779, https://doi.org/10.1029/1999GB900006, 1999.

Fourteau, K., Domine, F., and Hagenmuller, P.: Impact of water vapor diffusion and latent heat on the effective thermal conductivity of snow, The Cryosphere, 15, 2739-2755, https://doi.org/10.5194/tc-15-2739-2021, 2021.

Garge, N. R., Bobashev, G., and Eggleston, B.: Random forest methodology for model-based recursive partitioning: the mobForest package for R, BMC bioinformatics, 14, 125, https://doi.org/10.1186/1471-2105-14-125, 2013.

Goodarzi, M. R., Sabaghzadeh, M., Barzkar, A., Niazkar, M., and Saghafi, M.: A comparison of machine learning methods for estimation of snow density using satellite images, Water and Environment Journal, 38, 437-449, https://doi.org/10.1111/wej.12939, 2024.

Grünberg, I., Wilcox, E. J., Zwieback, S., Marsh, P., and Boike, J.: Linking tundra vegetation, snow, soil temperature, and permafrost, Biogeosciences, 17, 4261-4279, https://doi.org/10.5194/bg-17-4261-2020, 2020.

Gunn, M., Mills, J. S., Mahoney, M., Beier, C., Wen, T., and Tuttle, S. E.: A Machine Learning Approach for Snow Depth Estimation From Temperature Sensors, Hydrological Processes, 39, e70273, https://doi.org/10.1002/hyp.70273, 2025.

Hateffard, F., Steinbuch, L., and Heuvelink, G. B.: Evaluating the extrapolation potential of random forest digital soil mapping, Geoderma, 441, 116740, https://doi.org/10.1016/j.geoderma.2023.116740, 2024.

Jordan, R. E.: A one-dimensional temperature model for a snow cover: Technical documentation for SNTHERM. 89, 1991.

Joyce, J. M.: Kullback-leibler divergence, in: International encyclopedia of statistical science, Springer, 720-722, 2011.
Kanda, N. and Fletcher, C. G.: Evaluating a hierarchy of bias correction methods for ERA5-Land SWE across Canada, Environmental Research Communications, 7, 085015, https://doi.org/10.1088/2515-7620/aded5a, 2025.
King, J., Derksen, C., Toose, P., Langlois, A., Larsen, C., Lemmetyinen, J., Marsh, P., Montpetit, B., Roy, A., and Rutter, N.: The influence of snow microstructure on dual-frequency radar measurements in a tundra environment, Remote sensing of environment, 215, 242-254, https://doi.org/10.1016/j.rse.2018.05.028, 2018.
Krinner, G., Derksen, C., Essery, R., Flanner, M., Hagemann, S., Clark, M., Hall, A., Rott, H., Brutel-Vuilmet, C., and Kim, H.: ESM-SnowMIP: assessing snow models and quantifying snow-related climate feedbacks, Geoscientific Model Development, 11, 5027-5049, https://doi.org/10.5194/gmd-11-5027-2018, 2018.
Kullback, S.: Kullback-leibler divergence, Tech. Rep., 1951.
Lawrence, D. M., Fisher, R. A., Koven, C. D., Oleson, K. W., Swenson, S. C., Bonan, G., Collier, N., Ghimire, B., van Kampenhout, L., and Kennedy, D.: The Community Land Model version 5: Description of new features, benchmarking, and impact of forcing uncertainty, Journal of Advances in Modeling Earth Systems, 11, 4245-4287, https://doi.org/10.1029/2018MS001583, 2019.
Levasseur, S., Brown, K., Langlois, A., and McLennan, D.: Measurement of snow physical properties and stable isotope variations in the Canadian sub-Arctic and Arctic snowpack, Atmosphere-Ocean, 59, 137-151, https://doi.org/10.1080/07055900.2021.1962240, 2021.
Lin, J.: Divergence measures based on the Shannon entropy, IEEE Transactions on Information theory, 37, 145-151, 10.1109/18.61115, 1991.
Marsh, P., Bartlett, P., MacKay, M., Pohl, S., and Lantz, T.: Snowmelt energetics at a shrub tundra site in the western Canadian Arctic, Hydrological Processes, 24, 3603-3620, https://doi.org/10.1002/hyp.7786, 2010.
Mastepanov, M., Sigsgaard, C., Tagesson, T., Ström, L., Tamstorf, M., Lund, M., and Christensen, T.: Revisiting factors controlling methane emissions from high-Arctic tundra, Biogeosciences, 10, 5139-5158, https://doi.org/10.5194/bg-10-5139-2013, 2013.
Mavrovic, A., Sonnentag, O., Lemmetyinen, J., Voigt, C., Rutter, N., Mann, P., Sylvain, J.-D., and Roy, A.: Environmental controls of winter soil carbon dioxide fluxes in boreal and tundra environments, Biogeosciences, 20, 5087-5108, https://doi.org/10.5194/bg-20-5087-2023, 2023.
McGuire, A. D., Lawrence, D. M., Koven, C., Clein, J. S., Burke, E., Chen, G., Jafarov, E., MacDougall, A. H., Marchenko, S., and Nicolsky, D.: Dependence of the evolution of carbon dynamics in the northern permafrost region on the trajectory of climate change, Proceedings of the National Academy of Sciences, 115, 3882-3887, https://doi.org/10.1073/pnas.1719903115, 2018.
Meloche, J., Langlois, A., Rutter, N., McLennan, D., Royer, A., Billecocq, P., and Ponomarenko, S.: High-resolution snow depth prediction using Random Forest algorithm with topographic parameters: A case study in the Greiner watershed, Nunavut, Hydrological Processes, 36, e14546, https://doi.org/10.1002/hyp.14546, 2022.
Meløysund, V., Leira, B., Høiseth, K. V., and Lisø, K. R.: Predicting snow density using meteorological data, Meteorological Applications: A journal of forecasting, practical applications, training techniques and modelling, 14, 413-423, https://doi.org/10.1002/met.40, 2007.
Meyer, H. and Pebesma, E.: Predicting into unknown space? Estimating the area of applicability of spatial prediction models, Methods in Ecology and Evolution, 12, 1620-1633, https://doi.org/10.1111/2041-210X.13650, 2021.
Miner, K. R., Turetsky, M. R., Malina, E., Bartsch, A., Tamminen, J., McGuire, A. D., Fix, A., Sweeney, C., Elder, C. D., and Miller, C. E.: Permafrost carbon emissions in a changing Arctic, Nature Reviews Earth & Environment, 3, 55-67, https://doi.org/10.1038/s43017-021-00230-3, 2022.
Mudryk, L., Brown, R., Derksen, C., Luojus, K., Decharme, B., and Helfrich, S.: Terrestrial snow cover, https://doi.org/10.25923/16xy-9h55, 2019.
Mudryk, L., Santolaria-Otín, M., Krinner, G., Ménégoz, M., Derksen, C., Brutel-Vuilmet, C., Brady, M., and Essery, R.: Historical Northern Hemisphere snow cover trends and projected changes in the CMIP6 multi-model ensemble, The Cryosphere, 14, 2495-2514, https://doi.org/10.5194/tc-14-2495-2020, 2020.
Natali, S. M., Watts, J. D., Rogers, B. M., Potter, S., Ludwig, S. M., Selbmann, A.-K., Sullivan, P. F., Abbott, B. W., Arndt, K. A., and Birch, L.: Large loss of CO2 in winter observed across the northern permafrost region, Nature Climate Change, 9, 852-857, https://doi.org/10.1038/s41558-019-0592-8, 2019.
Pomarol Moya, O., Nussbaum, M., Mehrkanoon, S., Kraaijenbrink, P. D., Gouttevin, I., Karssenberg, D., and Immerzeel, W. W.: Improving snow water equivalent modelling: a comparative study of hybrid machine learning techniques, The Cryosphere, 20, 1427-1444, https://doi.org/10.5194/tc-20-1427-2026, 2026.
Pomeroy, J., Marsh, P., and Lesack, L.: Relocation of Major Ions in Snow along the Tundra-Taiga Ecotone: Paper presented at the 9th Northern Res. Basin Symposium/Workshop (Whitehorse/Dawson/Inuvik, Canada-August 1992), Hydrology research, 24, 151-168, https://doi.org/10.2166/nh.1993.0019, 1993.
Prasad, A., Merkouriadi, I., and Nummelin, A.: Modeling snow on sea ice using physics-guided machine learning, Environmental Data Science, 3, e28, https://doi.org/10.1017/eds.2024.40, 2024.

https://doi.org/10.5194/egusphere-2026-3363
Preprint. Discussion started: 20 July 2026

Proksch, M., Rutter, N., Fierz, C., and Schneebeli, M.: Intercomparison of snow density measurements: bias, precision, and vertical resolution, The Cryosphere, 10, 371-384, https://doi.org/10.5194/tc-10-371-2016, 2016.

Rantanen, M., Karpechko, A. Y., Lipponen, A., Nordling, K., Hyvärinen, O., Ruosteenoja, K., Vihma, T., and Laaksonen, A.: The Arctic has warmed nearly four times faster than the globe since 1979, Communications Earth & Environment, 3, 1-10, https://doi.org/10.1038/s43247-022-00498-3, 2022.

Revuelto, J., Billecocq, P., Tuzet, F., Cluzet, B., Lamare, M., Larue, F., and Dumont, M.: Random forests as a tool to understand the snow depth distribution and its evolution in mountain areas, Hydrological Processes, 34, 5384-5401, https://doi.org/10.1002/hyp.13951, 2020.

Rixen, C., Høye, T. T., Macek, P., Aerts, R., Alatalo, J. M., Anderson, J. T., Arnold, P. A., Barrio, I. C., Bjerke, J. W., and Björkman, M. P.: Winters are changing: snow effects on Arctic and alpine tundra ecosystems, Arctic Science, 8, 572-608, https://doi.org/10.1139/as-2020-0058, 2022.

Roberts, D. R., Bahn, V., Ciuti, S., Boyce, M. S., Elith, J., Guillera-Arroita, G., Hauenstein, S., Lahoz-Monfort, J. J., Schröder, B., and Thuiller, W.: Cross-validation strategies for data with temporal, spatial, hierarchical, or phylogenetic structure, Ecography, 40, 913-929, https://doi.org/10.1111/ecog.02881, 2017.

Romanovsky, V. E. and Osterkamp, T.: Effects of unfrozen water on heat and mass transport processes in the active layer and permafrost, Permafrost and Periglacial Processes, 11, 219-239, https://doi.org/10.1002/1099-1530(200007/09)11:3<219::AID-PPP352>3.0.CO;2-7, 2000.

Royer, A., Picard, G., Vargel, C., Langlois, A., Gouttevin, I., and Dumont, M.: Improved Simulation of Arctic Circumpolar Land Area Snow Properties and Soil Temperatures, Frontiers in Earth Science, 9, 515, https://doi.org/10.3389/feart.2021.685140, 2021.

Rutherford, J., Rutter, N., Wake, L., and Cannon, A. J.: Snow thermal conductivity controls future winter carbon emissions in shrub–tundra, Biogeosciences, 22, 5031-5049, https://doi.org/10.5194/bg-22-5031-2025, 2025.

Schimel, J. P., Bilbrough, C., and Welker, J. M.: Increased snow depth affects microbial activity and nitrogen mineralization in two Arctic tundra communities, Soil Biology and Biochemistry, 36, 217-227, https://doi.org/10.1016/j.soilbio.2003.09.008, 2004.

Schimel, J. P., Fahnestock, J., Michaelson, G., Mikan, C., Ping, C.-L., Romanovsky, V. E., and Welker, J.: Cold-season production of CO2 in arctic soils: can laboratory and field estimates be reconciled through a simple modeling approach?, Arctic, Antarctic, and Alpine Research, 38, 249-256, 2006.

Schuur, E. A., McGuire, A. D., Schädel, C., Grosse, G., Harden, J. W., Hayes, D. J., Hugelius, G., Koven, C. D., Kuhry, P., and Lawrence, D. M.: Climate change and the permafrost carbon feedback, Nature, 520, 171-179, 2015.

Serreze, M. C., Gustafson, J., Barrett, A. P., Druckenmiller, M. L., Fox, S., Voveris, J., Stroeve, J., Sheffield, B., Forbes, B. C., and Rasmus, S.: Arctic rain on snow events: bridging observations to understand environmental and livelihood impacts, Environmental Research Letters, 16, 105009, 10.1088/1748-9326/ac269b, 2021.

Slater, A. G., Lawrence, D. M., and Koven, C. D.: Process-level model evaluation: a snow and heat transfer metric, The Cryosphere, 11, 989-996, https://doi.org/10.5194/tc-11-989-2017, 2017.

Stuefer, S., Kane, D., and Dean, K.: Snow water equivalent measurements in remote Arctic Alaska watersheds, Water Resources Research, 56, e2019WR025621, 2020.

Stuefer, S. L., Hale, K., May, L. D., Mason, M., Vuyovich, C., Marshall, H.-P., Vas, D., and Elder, K.: Snow depth measurements from Arctic tundra and boreal forest collected during NASA SnowEx Alaska campaign, Scientific Data, 12, 919, 2025.

Sturm, M., Holmgren, J., and Liston, G. E.: A seasonal snow cover classification system for local to global applications, Journal of climate, 8, 1261-1283, https://doi.org/10.1175/1520-0442(1995)008<1261:ASSCCS>2.0.CO;2, 1995.

Sturm, M., Perovich, D. K., and Holmgren, J.: Thermal conductivity and heat transfer through the snow on the ice of the Beaufort Sea, Journal of Geophysical Research: Oceans, 107, SHE 19-11-SHE 19-17, 2002.

Sturm, M., Holmgren, J., König, M., and Morris, K.: The thermal conductivity of seasonal snow, Journal of Glaciology, 43, 26-41, https://doi.org/10.3189/S0022143000002781, 1997.

Sturm, M., Holmgren, J., McFadden, J. P., Liston, G. E., Chapin, F. S., and Racine, C. H.: Snow–shrub interactions in Arctic tundra: a hypothesis with climatic implications, Journal of Climate, 14, 336-344, 2001.

Thompson, A., Kelly, R., and Marsh, P.: Spatial variability of snow at Trail Valley Creek, NWT, 73rd Eastern Snow Conference, Columbus, Ohio, USA, 101-108,

Trenberth, K. E.: Atmospheric moisture residence times and cycling: Implications for rainfall rates and climate change, Climatic change, 39, 667-694, https://doi.org/10.1023/A:1005319109110, 1998.

Tutton, R., Dakin, B., Essery, R., Griffith, J., Hould-Gosselin, G., Marsh, P., Sonnentag, O., Thorne, R., and Walker, B.: A hydrometeorological dataset from the taiga-tundra ecotone in the western Canadian Arctic: Trail Valley Creek, Northwest Territories (V5), Borealis [dataset], doi:10.5683/SP3/BXV4DE, 2025.

van Kampenhout, L., Lenaerts, J. T., Lipscomb, W. H., Sacks, W. J., Lawrence, D. M., Slater, A. G., and van den Broeke, M. R.: Improving the representation of polar snow and firn in the Community Earth System Model, Journal of Advances in Modeling Earth Systems, 9, 2583-2600, 2017.

https://doi.org/10.5194/egusphere-2026-3363
Preprint. Discussion started: 20 July 2026

Vionnet, V., Leroux, N. R., Fortin, V., Abrahamowicz, M., Woolley, G., Mazzotti, G., Gaillard, M., Lafaysse, M., Royer, A., and Domine, F.: Enhancing simulations of snowpack properties in land surface models with the Soil, Vegetation and Snow scheme v2. 0 (SVS2), EGUsphere, 2025, 1-43, https://doi.org/10.5194/gmd-18-9119-2025, 2025.

Walker, B. and Marsh, P.: Snow depth, density, and snow water equivalent observations at Trail Valley Creek Research Station, Northwest Territories, 2015-2019 (V1), Borealis [dataset], https://doi.org/10.5683/SP2/RUSEHA, 2021.

Wang, H., Zhang, X., Xiao, P., Che, T., Zheng, Z., Dai, L., and Luan, W.: Towards large-scale daily snow density mapping with spatiotemporally aware model and multi-source data, The Cryosphere, 17, 33-50, https://doi.org/10.5194/tc-17-33-2023, 2023.

Webb, E. E., Schuur, E. A., Natali, S. M., Oken, K. L., Bracho, R., Krapek, J. P., Risk, D., and Nickerson, N. R.: Increased wintertime CO2 loss as a result of sustained tundra warming, Journal of Geophysical Research: Biogeosciences, 121, 249-265, https://doi.org/10.1002/2014JG002795, 2016.

Wilcox, E. J., Keim, D., de Jong, T., Walker, B., Sonnentag, O., Sniderhan, A. E., Mann, P., and Marsh, P.: Tundra shrub expansion may amplify permafrost thaw by advancing snowmelt timing, Arctic Science, 5, 202-217, 2019.

Woolley, G. J., Rutter, N., Wake, L., Vionnet, V., Derksen, C., Essery, R., Marsh, P., Tutton, R., Walker, B., and Lafaysse, M.: Multi-physics ensemble modelling of Arctic tundra snowpack properties, The Cryosphere, 18, 5685-5711, https://doi.org/10.5194/tc-18-5685-2024, 2024.

Woolley, G. J., Rutter, N., Wake, L., Vionnet, V., Derksen, C., Meloche, J., Montpetit, B., Leroux, N. R., Essery, R., and Hould Gosselin, G.: Simulating snow properties and Ku-band backscatter across the forest-tundra ecotone, EGUsphere, 2025, 1-37, 2025.

Yang, J., Jiang, L., Luojus, K., Pan, J., Lemmetyinen, J., Takala, M., and Wu, S.: Snow depth estimation and historical data reconstruction over China based on a random forest machine learning approach, The Cryosphere, 14, 1763-1778, https://doi.org/10.5194/tc-14-1763-2020, 2020.

Zhang, T.: Influence of the seasonal snow cover on the ground thermal regime: An overview, Reviews of geophysics (1985), 43, RG4002-n/a, 10.1029/2004RG000157, 2005.

Zhao, W., Fang, J., Yang, T., Lian, X., Winkler, A. J., Sun, F., and Gentine, P.: Observation-constrained physical snow water equivalent simulations using a physics-guided machine learning approach, Water Resources Research, 62, e2025WR041406, https://doi.org/10.1029/2025WR041406, 2026.

Zhao, W., Mu, C., Wu, X., Zhong, X., Peng, X., Liu, Y., Sun, Y., Liang, B., and Zhang, T.: Spatio-Temporal Characteristics and Differences in Snow Density between the Tibet Plateau and the Arctic, Remote Sensing, 15, 3976, https://doi.org/10.3390/rs15163976, 2023.

Zhao, Y., Nan, Z., Ji, H., and Zhao, L.: Convective heat transfer of spring meltwater accelerates active layer phase change in Tibet permafrost areas, The Cryosphere, 16, 825-849, 2022.

Zona, D., Gioli, B., Commane, R., Lindaas, J., Wofsy, S. C., Miller, C. E., Dinardo, S. J., Dengel, S., Sweeney, C., and Karion, A.: Cold season emissions dominate the Arctic tundra methane budget, Proceedings of the National Academy of Sciences, 113, 40-45, https://doi.org/10.1073/pnas.1516017113, 2016.